

MRI-guided Radiation Therapy: An Emerging Paradigm in Adaptive Radiation Oncology

Ricardo Otaño, PhD • Philippe Lambin, PhD • Jean-Philippe Pignol, MD, PhD • Mark E. Ladd, PhD • Heinz-Peter Schlemmer, MD, PhD • Michael Baumann, MD • Hedvig Hricak, MD, PhD

From the Departments of Medical Physics (R.O.) and Radiology (R.O., H.H.), Memorial Sloan-Kettering Cancer Center, 1275 York Ave, New York, NY 10065; The D-Lab, Department of Precision Medicine, Department of Radiology & Nuclear Medicine, GROW-School for Oncology, Maastricht University Medical Centre, Maastricht, the Netherlands (P.L.); Department of Radiation Oncology, Dalhousie University, Halifax, Canada (J.P.P.); Divisions of Medical Physics in Radiology (M.E.L.), Radiology (H.P.S.), and Radiation Oncology/Radiobiology (M.B.), German Cancer Research Center (DKFZ), Heidelberg, Germany; Faculty of Physics and Astronomy (M.E.L.) and Faculty of Medicine (M.E.L., M.B.), Heidelberg University, Heidelberg, Germany; and OncoRay—National Center for Radiation Research in Oncology, Faculty of Medicine and University Hospital Carl Gustav Carus, Technische Universität Dresden, Helmholtz-Zentrum Dresden-Rossendorf, Dresden, Germany (M.B.). Received July 13, 2020; revision requested August 6; revision received September 5; accepted September 9. **Address correspondence to** M.B. (e-mail: michael.baumann@dkfz.de).

R.O. and H.H. supported by the National Institutes of Health/National Cancer Institute (P30 CA008748).

Conflicts of interest are listed at the end of this article.

Radiology 2021; 298:248–260 • <https://doi.org/10.1148/radiol.2020202747> • Content codes:  

Radiation therapy (RT) continues to be one of the mainstays of cancer treatment. Considerable efforts have been recently devoted to integrating MRI into clinical RT planning and monitoring. This integration, known as MRI-guided RT, has been motivated by the superior soft-tissue contrast, organ motion visualization, and ability to monitor tumor and tissue physiologic changes provided by MRI compared with CT. Offline MRI is already used for treatment planning at many institutions. Furthermore, MRI-guided linear accelerator systems, allowing use of MRI during treatment, enable improved adaptation to anatomic changes between RT fractions compared with CT guidance. Efforts are underway to develop real-time MRI-guided intrafraction adaptive RT of tumors affected by motion and MRI-derived biomarkers to monitor treatment response and potentially adapt treatment to physiologic changes. These developments in MRI guidance provide the basis for a paradigm change in treatment planning, monitoring, and adaptation. Key challenges to advancing MRI-guided RT include real-time volumetric anatomic imaging, addressing image distortion because of magnetic field inhomogeneities, reproducible quantitative imaging across different MRI systems, and biologic validation of quantitative imaging. This review describes emerging innovations in offline and online MRI-guided RT, exciting opportunities they offer for advancing research and clinical care, hurdles to be overcome, and the need for multidisciplinary collaboration.

© RSNA, 2020

Online SA-CME • See www.rsna.org/learning-center-ry

Learning Objectives:

After reading the article and taking the test, the reader will be able to:

- Identify the major advantages and challenges of using MRI to guide radiation therapy (RT) procedures
- Describe the use of MRI for interfraction and intrafraction adaptation of RT with a combined MRI-guided linear accelerator (MRI-linac)
- Discuss the added value of physiologic MRI for treatment planning and response assessment

Accreditation and Designation Statement

The RSNA is accredited by the Accreditation Council for Continuing Medical Education (ACCME) to provide continuing medical education for physicians. The RSNA designates this journal-based SA-CME activity for a maximum of 1.0 AAMA PRA Category 1 Credit[®]. Physicians should claim only the credit commensurate with the extent of their participation in the activity.

Disclosure Statement

The ACCME requires that the RSNA, as an accredited provider of CME, obtain signed disclosure statements from the authors, editors, and reviewers for this activity. For this journal-based CME activity, author disclosures are listed at the end of this article.

Radiation therapy (RT) continues to be one of the mainstays of cancer treatment. Globally, more than 40% of patients with cancer undergo RT at least once for curative or palliative treatment (1). Over the years, the precision of treatment delivery has undergone both incremental and major advances (Fig 1). These advances have been enabled to a great extent by innovations in imaging guidance. In the 1990s, the use of three-dimensional CT imaging guidance and computers was a first major step into adaptive treatment (ie, the ability to change the treatment plan and the treatment delivery on the basis of imaging). This led to three-dimensional conformal RT, intensity-modulated RT, and stereotactic body RT planning, which have dramatically improved conformity of the dose distribution to the target volume, often reduced the irradiated volume, and improved outcomes. Another important development was the installment of imaging equipment such as orthogonal

radiography, CT, or linear accelerator-mounted cone-beam CT equipment directly in RT rooms. This has allowed frequent verification of the positioning of the tumor relative to nearby critical normal tissues and of the planned dose distribution. Image-guided intensity-modulated RT has increasingly become a standard of care for high-dose clinical RT.

More recently, considerable research efforts have been devoted to the integration of MRI into the RT workflow. The move toward this approach, known as MRI-guided RT, has been motivated by the superior soft-tissue contrast, improved organ motion visualization, and enhanced capacity for imaging of tissue and tumor physiologic structure provided by MRI compared with CT.

Clinical implementation of MRI-guided RT has already begun with the use of offline MRI (outside the treatment session) for treatment planning, for example, in patients

This copy is for personal use only. To order printed copies, contact reprints@rsna.org

Abbreviations

CEST = chemical exchange saturation transfer, DCE = dynamic contrast enhanced, MRI-linac = MRI-guided linear accelerator, RT = radiation therapy

Summary

The integration of MRI and linear accelerators is revolutionizing cancer treatments, offering possibilities to adapt radiation therapy with greater precision and in real time to account for anatomic and physiologic changes, and monitor treatment response.

Essentials

- Offline MRI-guided radiation therapy (RT; outside the treatment session) is already used for treatment planning, and several studies have demonstrated its promise for assessment of treatment response.
- Online MRI-guided RT (during the treatment session) by using hybrid MRI-guided linear accelerator systems is an emerging technology, offering unprecedented opportunities for interfraction and real-time intrafraction adaptation to organ motion and calculation of dose accumulation.
- The use of MRI in RT promises to lead to better understanding and monitoring of tumor biology during radiation treatment and ultimately the development and application of a generation of imaging biomarkers for tumor response.
- Challenges to MRI-guided RT include real-time volumetric anatomic imaging, reproducible quantitative imaging across different MRI systems, and biologic validation of quantitative imaging.
- To overcome the above challenges and facilitate advances in patient care, it is imperative that the radiology and radiation oncology communities work closely together, recognizing the importance of the ongoing convergence of life sciences, physical sciences, and engineering for enabling rapid innovation.

with prostate (2) and head and neck (3) cancers. Now, MRI-guided linear accelerator (MRI-linac) systems—which combine MRI with a linear accelerator—are being used, providing an online MRI platform for treatment planning, adaptation, and monitoring during a treatment session (Table) (4–8). Figure 2 shows the general idea of using online MRI-guided RT for interfraction and intrafraction adaptation to organ motion. Online MRI-guided RT offers opportunities for real-time adaptive treatment within each fraction in tumors affected by continuous motion (eg, tumors in the lungs, kidneys, liver, pancreas, and neck) and by sporadic motion (eg, tumors in the prostate and rectum). The idea of adapting RT to changes identified at imaging is not new or unique to MRI. However, the advantages of MRI over CT are expected to significantly improve the ability to adapt to changes over the entire course of treatment, including within treatment sessions. The current focus of online MRI-guided RT is adaptation to anatomic changes. In the longer term, biomarkers derived from quantitative MRI techniques are expected to enable adaptation to physiologic structure and treatment response.

The purpose of our review is to describe recent clinical developments in MRI-guided RT and opportunities the technology offers for improving cancer care and research. It also addresses key challenges that need to be overcome and the importance of multidisciplinary collaboration for realizing the potential of MRI-guided RT. The intended readership includes both

clinicians and developers: Current advantages and potential benefits are described for clinicians, and challenges are presented for developers.

Offline MRI-guided RT

In offline MRI simulation, which is already playing an increasing role in treatment planning, the immobilization device that will be used at treatment delivery is used to position the patient as closely as possible to (ie, to simulate) the treatment position (9,10). Though MRI compatible, the immobilization device can cause signal-to-noise ratio loss because of increased distance between the receiver coil and the patient. Significant efforts are underway to develop flexible receiver coils that can be inserted between the immobilization device and patient to increase signal-to-noise ratio (11,12). An important development for MRI implementation in RT has been the application of pseudo-CT density data and synthetic CT, which allows MRI-only treatment planning by using Hounsfield units preassigned to each voxel (13–15). Figure 3 shows the application of MRI-only simulation with synthetic CT for prostate treatment planning. Compared with CT, MRI enables better visualization of the intraprostatic anatomy and better definition of the glandular prostate tissue within the periprostatic fat. MRI also provides access to information on physiologic characteristics, such as diffusion and perfusion, that can provide additional guidance for tumor delineation. The use of physiologic MRI information may also lead to dose painting of the part of the tumor likely to be the most radioresistant. There are clinical MRI-only simulation tools for treatment planning that are currently available, such as MRI for Calculating Attenuation (14).

High-accuracy offline MRI treatment planning requires addressing geometric distortions, which can be system dependent or patient dependent. System-dependent distortions originate from hardware imperfections such as gradient nonlinearities, main magnetic field (B_0) inhomogeneities, and eddy currents. These are measured by the manufacturer and can be corrected with image processing algorithms. The main source of system-dependent distortions is magnetic field gradient nonlinearities, which cause image warping that increases with the distance from isocenter. Large field-of-view or off-isocenter imaging can be challenging for correction algorithms to handle. Patient-dependent distortions are more complicated to address, because each patient has a unique set of magnetic properties. Correction of patient-dependent distortions would require the acquisition of calibration data from each patient, such as a B_0 map, and the use of a model-based reconstruction algorithm that incorporates the magnetic model of each patient (16).

System-dependent geometric distortion is usually measured weekly as part of a routine quality assurance procedure by using a phantom with a known grid structure. In this procedure, geometric distortion is defined as the shift of a point with respect to its reference position and is evaluated for several distances with respect to the isocenter. Different geometric distortion measures can be found in the literature depending on the scanner hardware, MRI sequence, and distortion correction algorithm (17). For highly accurate planning near critical structures, geometric distortions must be smaller than 1 mm. This is usually feasible

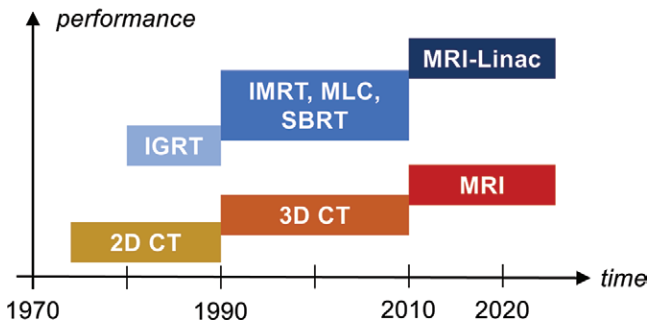


Figure 1: Evolution of image-guided radiation therapy (RT) methods (in blue shades) and corresponding imaging technique used for guidance (yellow, orange, red). IGRT = image-guided RT, IMRT = intensity-modulated RT, MLC = multileaf collimator, MRI-Linac = MRI-guided linear accelerator, SBRT = stereotactic body RT, 3D = three-dimensional, 2D = two-dimensional.

with MRI techniques that are less sensitive to B_0 inhomogeneities and correction algorithms that model gradient nonlinearities and magnetic field inhomogeneities. Immobilization devices are MRI transparent and thus they do not affect geometric distortion.

A more recent development in offline MRI-guided RT is the application of artificial intelligence methods for automatic structure identification and segmentation in treatment planning. These methods mitigate the time-consuming and labor-intensive aspects of manual contour delineation of the target and organs at risk and, at the same time, reduce inter- and intraobserver variability in contour delineation (18,19).

Online MRI-guided RT

Harold Johns, an influential physicist from the Ontario Cancer Institute and a pioneer in the use of Cobalt-60, once stated, “if you can’t see it, you can’t hit it, and if you can’t hit it, you can’t cure it” (20). Though this quote is not applicable to all types of cancer treatments, in particular to nonlocalized therapies, the ability to view the tumor and organs at risk before and during treatment is essential for effective and safe RT procedures. Today, the majority of RT systems include cone-beam CT, which enables visualization of tumors and nearby structures, allowing for more precise therapy for target volumes and organs (21,22). However, cone-beam CT in its current form has some important disadvantages: Because of photon scattering, it yields relatively poor soft-tissue contrast and poor image quality. In addition, it irradiates large volumes of tissues at a low dose in the range of 10 mSv per image, which limits continuous acquisition and hence prevents intrafraction motion assessment (23,24). These effects are particularly important when trying to adapt treatment to tumor motion, which requires implanted fiducial markers to follow target position with cone-beam CT (25,26). Recently, MRI-linac systems that combine an MRI system with a linear accelerator have been unveiled globally with the promise of overcoming the main limitations of cone-beam CT with respect to anatomic imaging and adding the potential of physiologic imaging. Several types of commercial or research MRI-linacs are already available (Table) (27). Current clinically approved systems are limited to coplanar irradiation because of the system geometry. The MRI system can have

any of various magnetic field strengths (from 0.35 T to 1.5 T). Lower magnetic fields minimize radiation dose distortion but have lower image quality because of decreases in signal-to-noise ratio.

The improved soft-tissue contrast of MRI allows for better lesion delineation for treatment without the use of a contrast agent; this has been shown for hepatic lesions, prostate, nasopharynx, rectal, and brain tumors (27,28). Figure 4 shows adaptation to interfraction anatomic changes in a patient with rectal cancer, where the ability to adapt treatment to the exact location and size of the tumor improved outcome and resulted in tumor remission. The MRI-linac also offers the advantage of improved visualization of organs at risk, with possibilities for avoiding so-called geographic misses while also reducing uncertainty margins. Figure 5 shows interfraction motion of organs at risk (liver, bowel, kidney, stomach, and duodenum) in a patient with pancreatic cancer; the ability to adapt treatment on the basis of imaging of interfraction motion enabled the use of high radiation doses with low toxicity levels.

One of the main promises of the MRI-linac is to enable real-time intrafraction adaptive RT of tumors affected by motion without the need for fiducials. This innovation would not only further decrease the risk of missing tumor cells, but in principle would also further reduce toxicity and therefore enable escalation of the radiation dose and use of fewer fractions. Ablative doses (on the order of biologic equivalent doses of 100 Gy) have been demonstrated to lead to unprecedented survival durations in patients with locally advanced unresectable pancreatic cancer (29). A first solution for real-time adaptation to motion is gating, where motion is continuously imaged at high temporal resolution and radiation is only delivered when the tumor is at a specific location. The group at the Amsterdam University Medical Center demonstrated single-fraction motion-gated lung stereotactic ablative RT in a cohort of 10 patients by using the ViewRay MRI-linac system (30) (Fig 6). However, because radiation is only delivered during a small fraction of the motion cycle, the overall treatment is elongated. In the case of single-fraction treatment of lung cancer, the average procedure time was about 2 hours. An alternative and potentially more efficient solution is multileaf collimator tracking. The multileaf collimator is a metallic device located between the x-ray source and the patient. It is composed of several leaves that can move independently, and it is used to rapidly reshape the radiation beam or to vary its intensity before it is delivered to the patient. For example, the multileaf collimator from the Elekta MRI-linac system has a latency (ie, delay between the command and the resulting displacement) of only about 20 msec (31). It needs to be stressed, however, that current MRI technology is relatively slow to image volumetric organ motion in real time. At the time that we are writing this article, even with the latest acquisition and reconstruction techniques, real-time MRI is limited to two-dimensional imaging, which has suboptimal interpretation of motion and through-plane motion misregistration. A significant effort is underway to develop real-time three-dimensional MRI techniques that are tailored to the needs of the MRI-linac and minimize imaging latency (the delay between the start of data acquisition and the end of image reconstruction). These

Table 1: Online MRI-guided Radiation Therapy Pioneer Systems

MRI Type	Specifications	Hospital*
0.35-T MRI whole-body scanner; 70-cm bore	6-MV linear accelerator	FDA-501 (k) cleared. Washington University, St Louis, MO (Mutic et al; 5)
1.5-T MRI scanner; Philips Achieva; 70-cm bore	7-MV linear accelerator (Elekta)	FDA-501 (k) cleared. University Medical Center Utrecht, Utrecht, Netherlands (Raaymakers et al; 6)
0.6-T MRI scanner; 60-cm gap	6-MV linear accelerator (research system)	Prototype at Cross Cancer Institute, Edmonton, Canada (Fallone et al; 7)
1-T MRI scanner; 50-cm gap	6-MV linear accelerator (design study)	Liverpool, Sydney, Australia (Keall et al; 8)

Note.—The irradiating source is high-energy x-rays, and the imaging units can have various magnetic fields strengths (from 0.35 to 1.5 T). FDA = Food and Drug Administration.

*Information in parentheses is first installation.

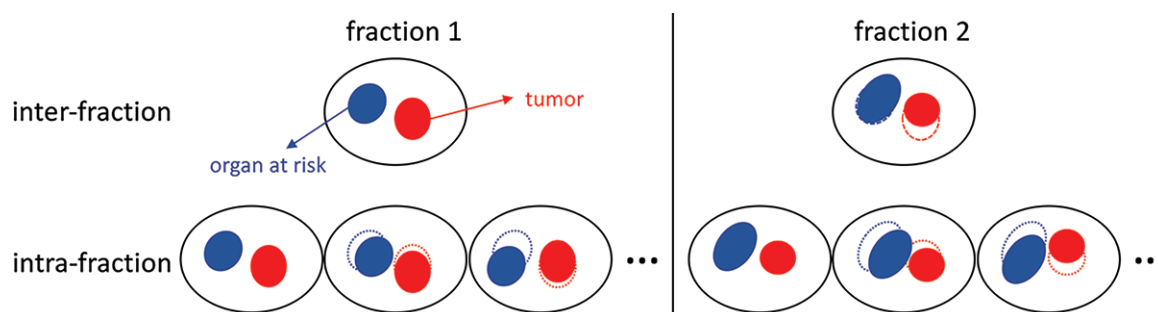


Figure 2: Schematic description of interfraction and intrafraction adaptation to organ motion by using online MRI-guided radiation therapy with a hybrid MRI-guided linear accelerator system. For interfraction adaptation, treatment is adjusted according to the image of the day (dashed lines show the position of the tumor and organ at risk for fraction 1). Intrafraction adaptation uses real-time imaging to adjust treatment according to continuous and/or sporadic organ motion within each fraction (dotted lines show the position of the tumor and organ at risk for the first point of real-time imaging).

techniques shift the acquisition and computational burden to an offline training (beam-off) phase at the start of each treatment fraction and leave simple operation for the online (beam-on) phase. For example, MR Signature Matching, or MRSIGMA, precomputes a dictionary of high-spatial-resolution three-dimensional motion states during treatment planning and uses fast acquisitions during the treatment delivery phase to match a dictionary entry in real time for each fraction (32). Figure 7 shows real-time three-dimensional motion imaging of a liver tumor by using MRSIGMA. MR Model-based Reconstruction of Motion from Undersampled Signals (33) precomputes an initial motion model, which is updated in real time by using a small amount of new data. These techniques, given their short acquisition times, could both be used for multileaf collimator tracking. Figure 8 illustrates the concept of the use of real-time three-dimensional MRI techniques for multileaf collimator tracking, which will enable adaptation to volumetric position and shape.

Another main advantage of obtaining accurate volumetric imaging during treatment would be the ability to calculate the accumulation of radiation dose in the tumor and in the organs at risk for each fraction. Accurate volumetric mapping of dose accumulation would allow interfraction, or even intrafraction, treatment adaptation if the tumor coverage or the organs-at-risk constraints are violated (34,35). It is well recognized that radiation damage in a given element of a specific tissue depends on total dose, dose per fraction, the time interval between the fractions, and overall treatment time and radiation beam quality

(36,37). Furthermore, the volume of the specific tissue or organs irradiated, and the exact dose distribution in these organs and their specific substructures (eg, in pericardium, muscle, arteries, valves, and the conduction system instead of simply the heart), are important determinants for the development of radiation damage (38,39). Making the voxel-by-voxel daily dose accumulation available would be helpful for deciding on the next fraction in a given patient, especially in the emerging context of treatments with few high-dose fractions. It would also allow the generation of detailed data regarding normal tissue tolerance, which would further advance evidence-based RT prescription and planning. The introduction of the MRI-linac has provided, to our knowledge, for the first time the potential to analyze radiation effects on tissues by continuously imaging the exact location of subvolumes of organs during beam-on time (40).

One of the major concerns in online MRI-guided RT is the so-called electron return effect. In this phenomenon, electrons in a magnetic field move in a circular pattern at inhomogeneous anatomic sites such as air-tissue interfaces and cause a dose increase in the higher-density medium. Radiation dose is mainly delivered by secondary electrons that carry the energy transferred from the initial beam. Secondary electrons deposit energy downstream in segments of straight lines. In the magnetic field, however, the path of the secondary electron is altered because of the Lorentz force. When the electron is generated in a dense medium and travels into a less dense medium, the electron is able to follow a circular path back into the original medium. Because of the lack of the

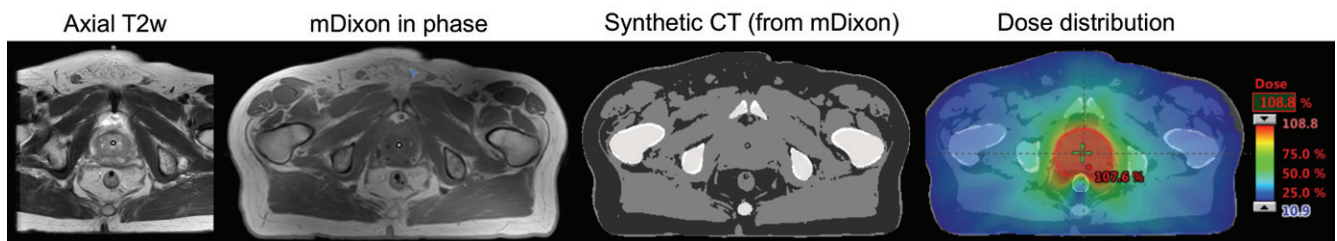


Figure 3: Offline MRI-guided RT of a patient with prostate cancer. The axial T2-weighted (T2w) image is used for diagnostic purposes, and the modified Dixon (mDixon) in-phase image is used for treatment planning. A synthetic CT image is created with an artificial intelligence algorithm from the mDixon image and is then used to compute the dose distribution. Figure adapted, with permission, from Dr Neelam Tyagi, Memorial Sloan-Kettering Cancer Center.

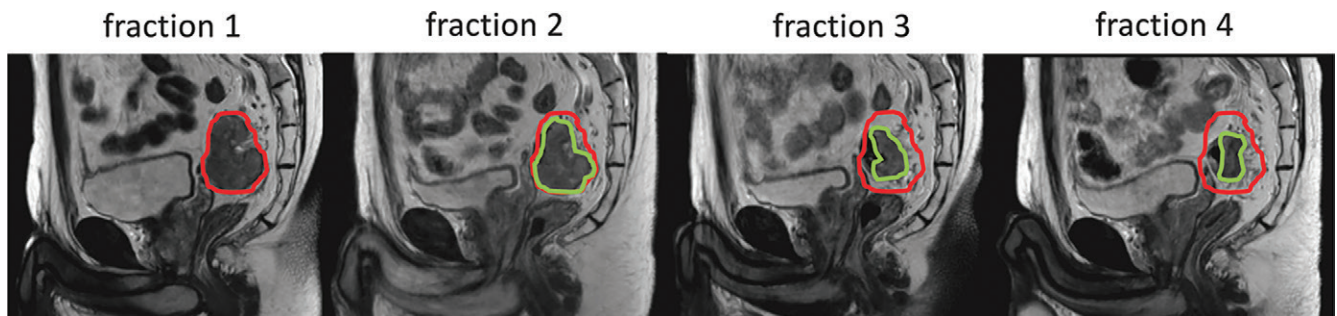


Figure 4: Interfraction adaptive treatment of a patient with rectal cancer on the Elekta 1.5T MRI-guided linear accelerator. Tumor contour for fraction 1 is shown in red and tumor contours for other fractions are shown in green. The ability to adapt treatment to the exact location and size of the tumor improved outcome and resulted in tumor remission. Figure adapted, with permission, from Drs Martijn In'tven and Bas Raaymakers, University Medical Center Utrecht.

electronic equilibrium, dose is increased in the original medium near the interface. In the Monte Carlo simulations and the film measurements performed by the Utrecht group, the electron return effect is observed to enhance dose at the interface by up to a factor of 1.3–1.4, over a range of about 1 cm (41). The same group also concluded these effects would be minimized by using multiple fields and could be macroscopically considered by Monte Carlo–based treatment planning procedures (42).

Quantitative MRI-derived Biomarkers from Treatment Response Assessment to Personalized RT

Though MRI was not originally conceived as a quantitative imaging technique, several quantitative biomarkers derived from MRI have been shown to reflect response to RT earlier than anatomic imaging features (43). Moreover, it is increasingly recognized that interpatient heterogeneity requires biomarker-based strategies toward personalized radiation oncology (44). MRI may provide new insights on the treatment response of both tumors and normal tissues in individual patients, which may serve to develop prognostic and potentially even predictive biomarkers. Among modern biotechnologies, only imaging can show longitudinal and spatially resolved information on dynamic biologic processes and the *in vivo* distribution of biomarkers. Here we present the application of promising MRI-derived biomarkers to assess treatment response.

Dynamic contrast–enhanced (DCE) MRI characterizes tumor microvasculature and has been clinically demonstrated to be useful for tumor diagnosis and treatment assessment (45). Pharmacokinetic analysis of DCE MRI models the transfer of the contrast agent, such as gadolinium chelate, between the vascular space and the extravascular extracellular space. Perfusion

and permeability parameters derived from DCE MRI, such as forward volume transfer constant, or K^{trans} , and reverse volume transfer constant, or k_{ep} , are consistently linked with tumor response to radiation on various anatomies. For example, K^{trans} derived from DCE MRI achieved 100% sensitivity and 83% specificity in detecting recurrent gliomas from radiation necrosis (46). K^{trans} and k_{ep} also correlated well with tumor regression, showing that tumors with increased perfusion and permeability have a better response to RT (47).

Another form of MRI, diffusion-weighted imaging, images the random Brownian motion of water molecules. The apparent diffusion coefficient calculated from diffusion-weighted imaging is a biomarker for tissue cell density. In healthy tissue, water molecules move freely and have high apparent diffusion coefficient values. However, in tumor tissue, diffusion is restricted, which causes a decrease in apparent diffusion coefficient values. Longitudinal studies that use diffusion-weighted imaging have shown increases in apparent diffusion coefficient values for responding head and neck (48) and prostate tumors (49) earlier than conventional anatomic imaging.

MRI signal relaxation parameters such as T1 and T2 can also be used to measure tumor cell density. T1 is the time constant for the magnetization recovery along the z-axis and T2 is the time constant for the magnetization decay in the x-y plane. Tumors have elevated T1 and T2 values. T2 mapping was successfully demonstrated to help predict response to RT in prostate cancer, particularly in the peripheral zone, where a consistent decrease of T2 was observed at week 6 from a total of 8 weeks of treatment (50).

Chemical exchange saturation transfer (CEST) MRI indirectly helps to measure mobile protein and peptide content in

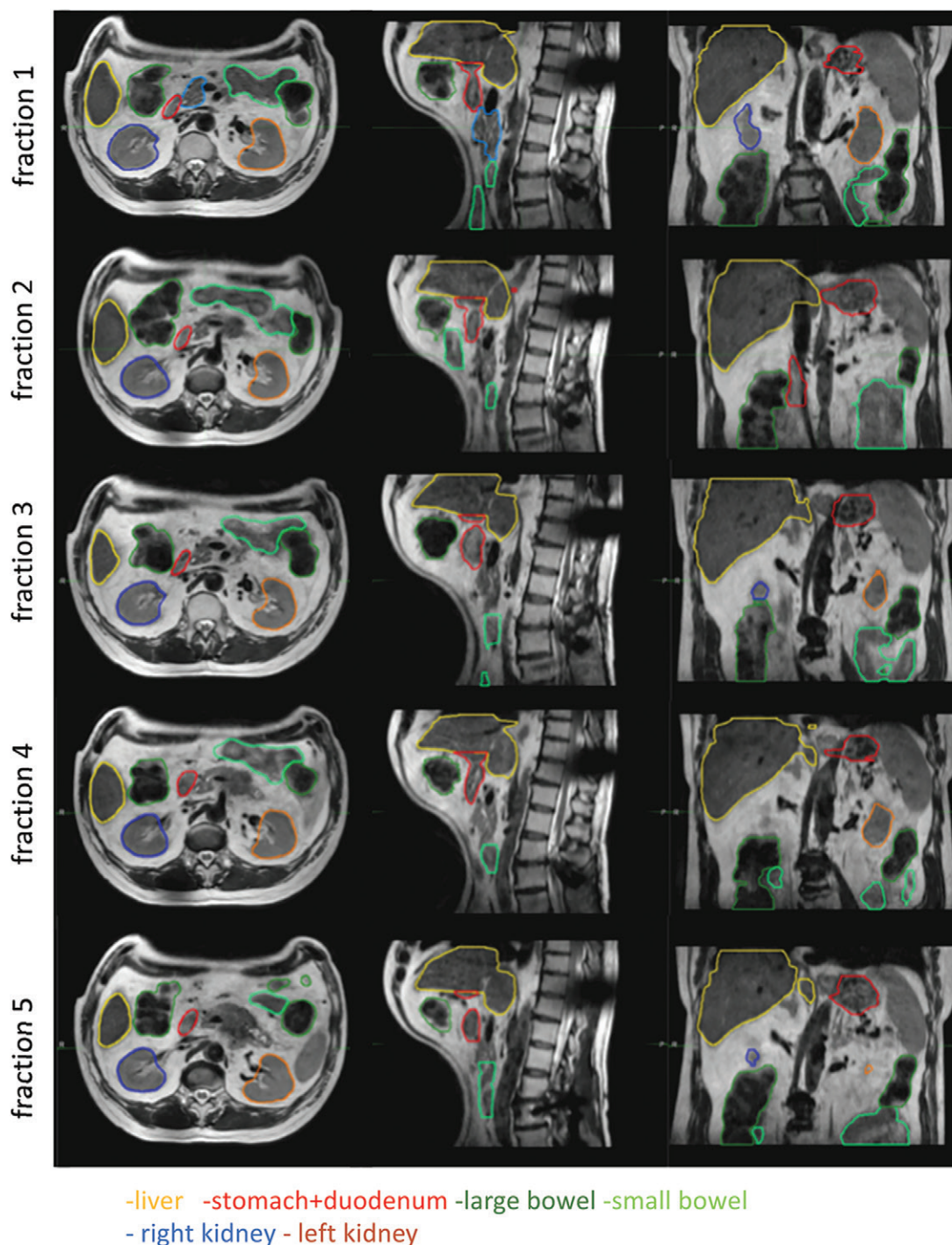


Figure 5: Interfraction motion of organs at risk (liver, bowel, kidney, stomach, and duodenum) in a patient with pancreas cancer undergoing five-fraction stereotactic body radiation treatment (10 Gy \times 5) on the Elekta 1.5-T MRI-guided linear accelerator. The ability to adapt treatment according to the position of the organs at risk increased safety of the procedure. Figure used, with permission, from Dr Neelam Tyagi, Memorial Sloan-Kettering Cancer Center.

tissue by depicting endogenous biomolecules that possess protons that can undergo exchange with water molecules (51). Protein content is higher in areas of elevated cellular density and proliferation, which are increased in aggressive tumors. CEST may be informative to monitor early effects of RT, which results in destruction of the cytoplasm, increasing the mobile protein content. Decreases in mobile protein content with CEST may

be observed at earlier points than decreases in tissue cellularity assessed at diffusion MRI. Amide proton transfer CEST was demonstrated to distinguish true progression from pseudoprogression in patients with glioma who underwent radiation treatment (52).

CEST also demonstrated potential to determine tumor hypoxia without use of PET tracers by measuring acidic extracellular

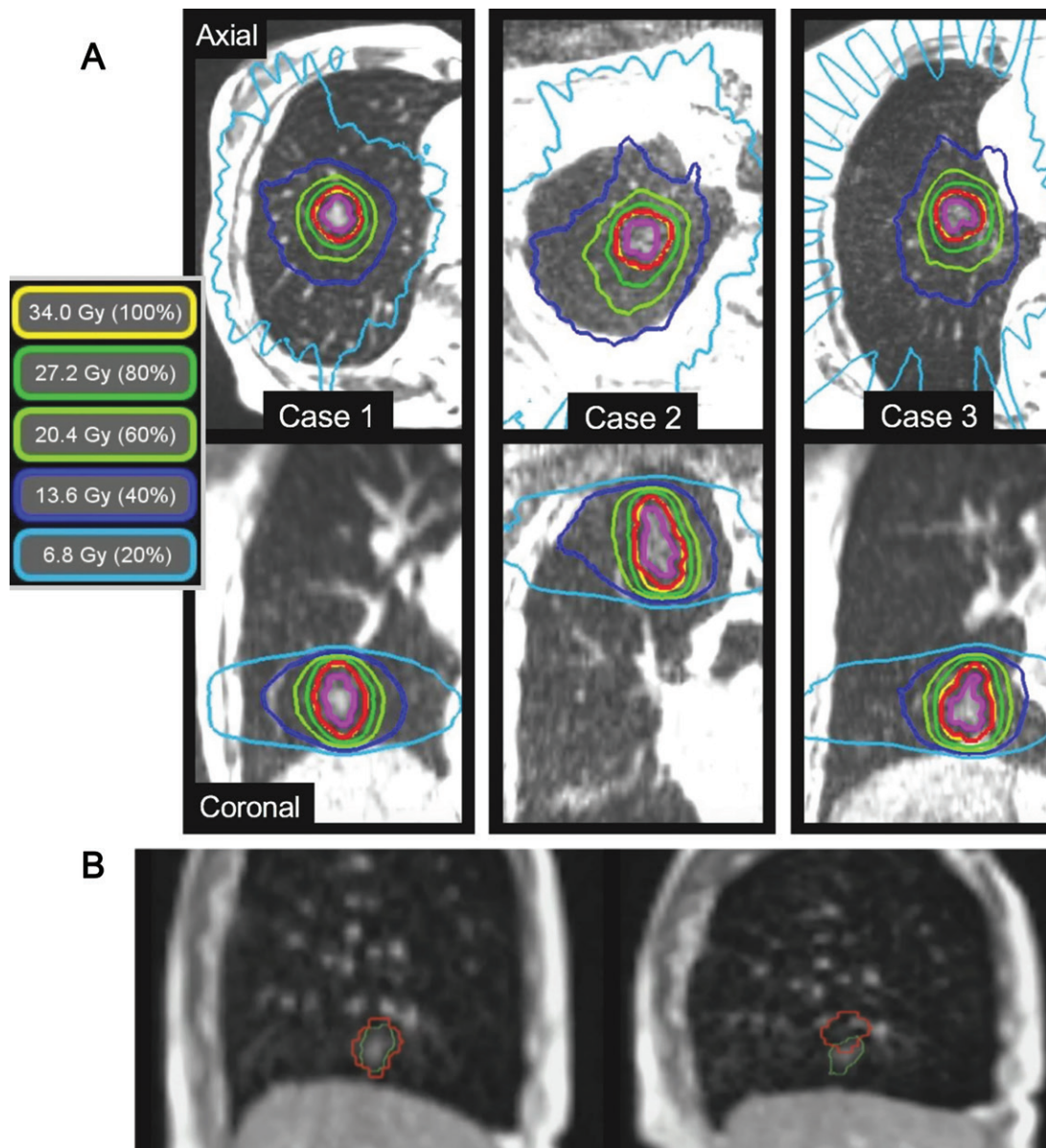


Figure 6: Single-fraction motion-gated lung stereotactic ablative radiation therapy by using the ViewRay 0.35-T MRI-guided linear accelerator system. A, Treatment plan for the first three patients, where one fraction of 34 Gy is delivered to the planning target volume (red). The planning target volume is created by adding a 5-mm isotropic margin to the breath-hold gross tumor volume (purple). B, Real-time two-dimensional motion tracking of the gross tumor volume (green) in one of the patients, which is performed by using two-dimensional images acquired in sagittal orientation every 250 msec and deformable image registration. During delivery, the beam is automatically turned off when a specified proportion of the gross tumor volume is outside the gating window (red). In B, on the left-hand image the full gross tumor volume is contained within the gating window, whereas on the right-hand image, about 75% of the gross tumor volume is outside the gating window. Modified, with permission, from reference 30.

pH (53). Hypoxic tumors are more radioresistant than tumors with higher oxygenation (54,55). Tumor hypoxia is neither distributed homogeneously throughout individual tumors nor constant during the course of RT, as demonstrated by PET imaging with hypoxia tracers such as fluorine 18 (^{18}F) misonidazole or ^{18}F -HX4. CEST is limited to high-field-strength MRI, and whether similar techniques or ultrasensitive hypoxia-specific contrast materials can be developed for MRI at the magnetic field strengths used in MRI-linacs needs to be explored (56,57). Another MRI technique that could be applied for imaging of hypoxia is blood oxygenation level-dependent imaging relying on the difference in

the paramagnetic properties of oxyHb and deoxyHb (58). Imaging of tumor perfusion with DCE MRI represents still another way to image hypoxia and therefore radioresistance; it already has clinical applications in a variety of tumors from several parts of the body (59). The effect of oxygen on treatment planning and treatment response can be analyzed by using the oxygen enhancement ratio, which is defined as the ratio of radiation dose with hypoxia and radiation dose with full oxygenation to achieve the same level of cell damage (60). At full oxygenation, the oxygen enhancement ratio is unity. Its value increases with decreasing oxygen concentration to a maximum of 2.7. This suggests the radiation dose at a

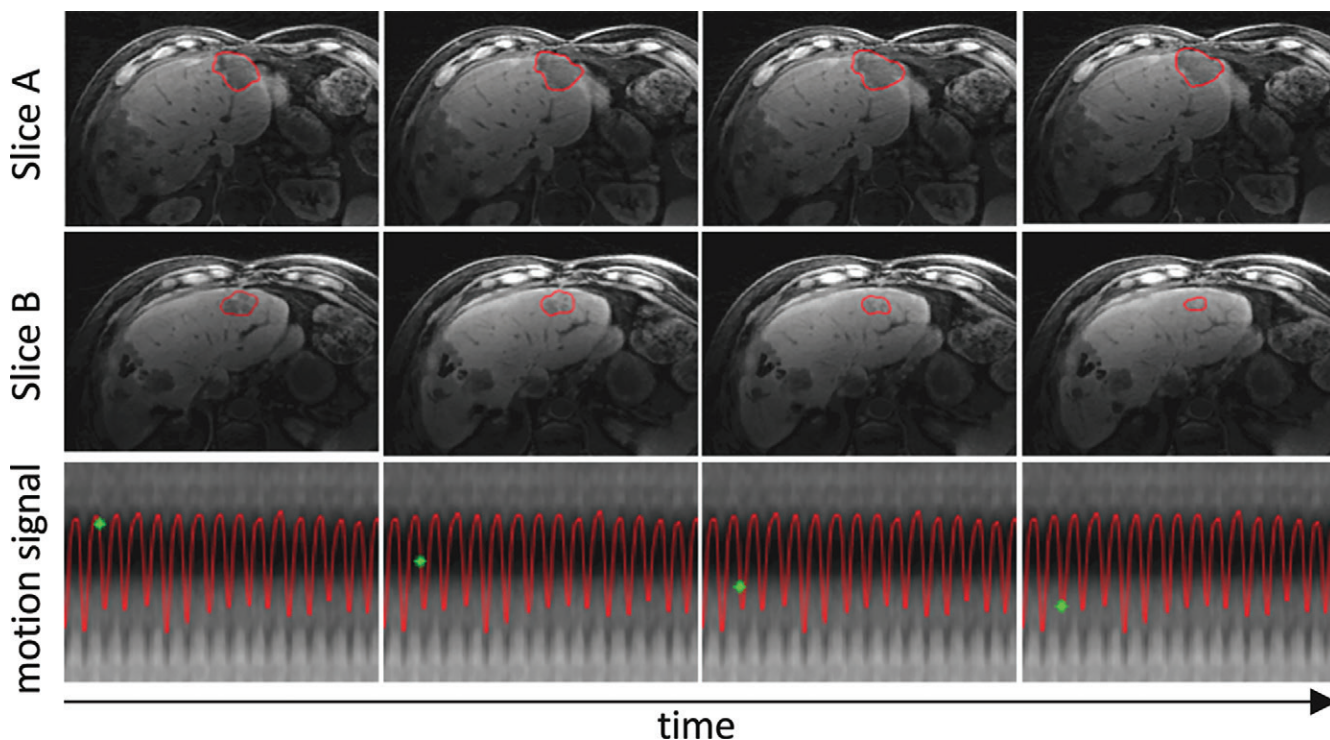


Figure 7: Real-time volumetric liver tumor motion tracking by using the MR Signature Matching technique for two representative sections. The tumor contour is shown in red. The motion-signal row shows the temporal location (green point) in the respiratory motion signal. Total imaging latency including data acquisition and image reconstruction for each three-dimensional image is about 250 msec. Access to real-time volumetric motion information would in principle allow continuous adaptation of the radiation beam to the tumor motion.

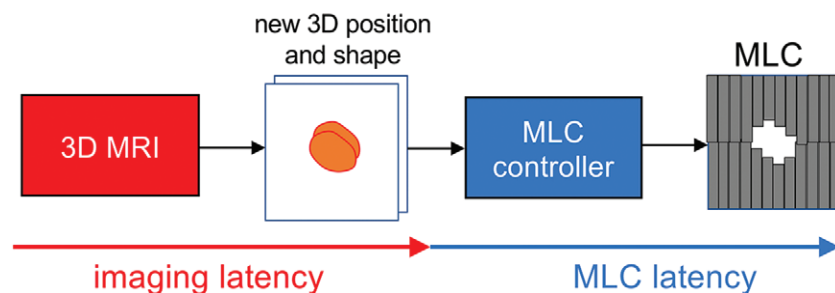


Figure 8: General idea for real-time three-dimensional MRI-guided intrafraction adaptive-to-shape treatment. A fast three-dimensional (3D) MRI technique will provide the volumetric position and shape of the target, which will be streamed to the multileaf collimator (MLC) controller. The MLC controller will adapt to the volumetric position and shape by moving the multiple leaves. The tracking latency (ie, the time from the start of image acquisition to the end of multileaf collimator movement) is provided by the sum of imaging latency (including acquisition, reconstruction, and segmentation) and multileaf collimator latency. Developments in fast three-dimensional MRI are aimed at minimizing the imaging latency for real-time three-dimensional adaptation.

region without oxygen has to be 2.7-fold higher than the one at a well-oxygenated region. Oxygen enhancement ratio is not linear with oxygen concentration and rather follows a hyperbolic curve. Beyond oxygen partial pressures of 20 mm Hg, no additional treatment benefit is obtained by increasing oxygen concentration, at least for the atmospheric pressure. MRI-based hypoxia measurements together with the oxygen enhancement ratio model can potentially be used to prescribe higher doses in hypoxic regions. Targeting hypoxic regions can also improve immunotherapy, and a combination of RT and immunotherapy can be used to improve treatment outcomes (61).

In addition to being a promising biomarker for hypoxia, CEST has demonstrated potential for noninvasive identification of patients with superior prognostic characteristics by yielding results that correlate well with histopathologic findings. Figure 9 shows the application of CEST for predicting histopathologic parameters in recently diagnosed untreated glioma (62).

Measurements of tumor nore lactate content and distribution by using MR spectroscopy are another avenue for prediction of RT response because a close association exists between tumor lactate levels and radioresistance (63,64). The major drawback of MR spectroscopy for clinical application is its low sensitivity. As a potential means to overcome

this problem, hyperpolarized metabolic substrates have elicited increasing interest. In particular, imaging of hyperpolarized ^{13}C -pyruvate is currently on a path toward clinical translation (65–67).

In recent years, a new direction in cancer research, referred to as radiogenomics or imaging genomics, has emerged (68). Radiogenomics focuses on the relationship between imaging phenotypes and genomic characteristics of a tumor (the term *radiogenomics* may also refer to a separate area of study that links genetic features with radio-sensitivity, but that area of research is not discussed here). Several studies have shown that certain genes are associated

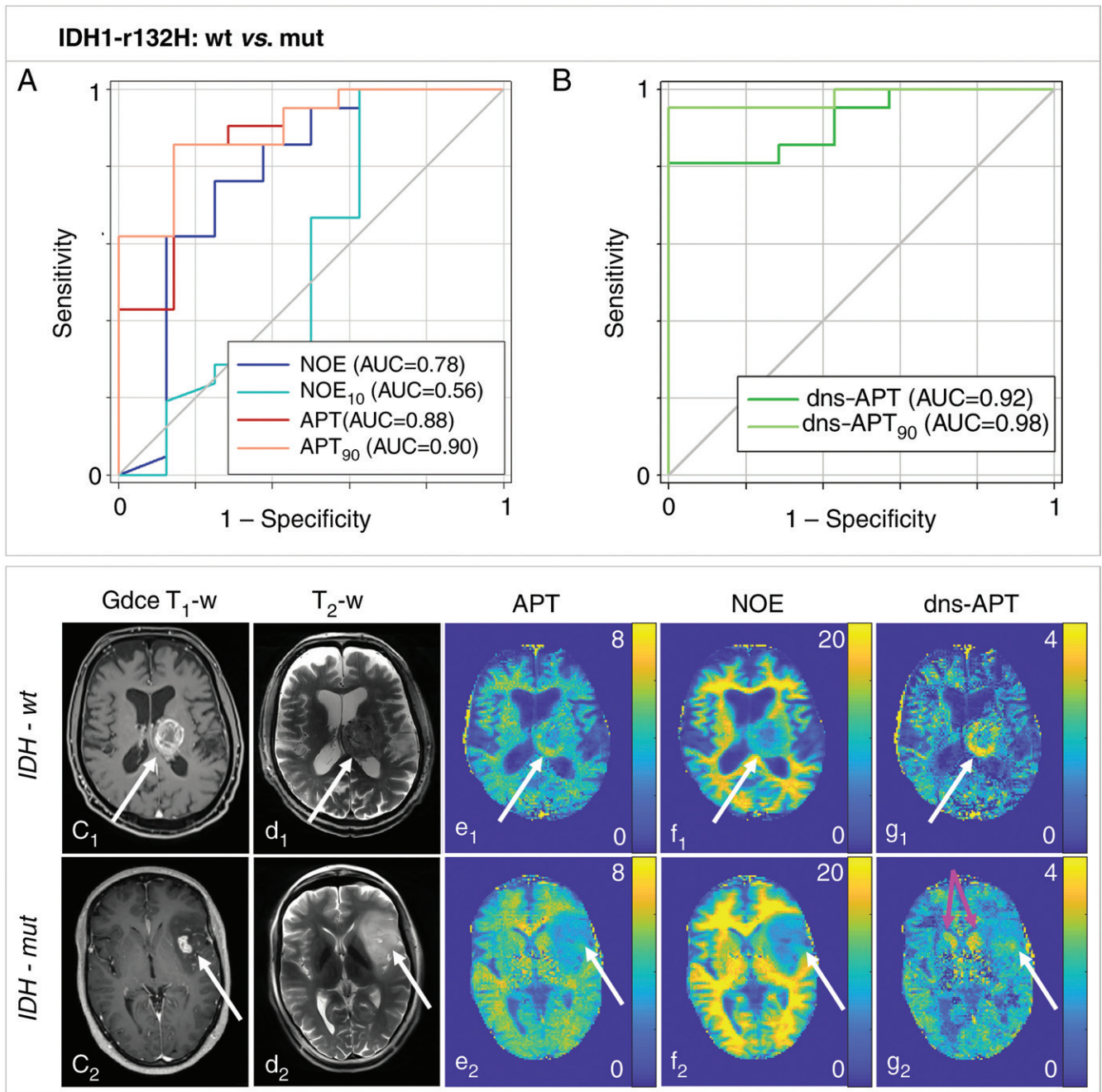


Figure 9: Chemical exchange saturation transfer (CEST) MRI can noninvasively help to predict histopathologic characteristics to help identify patients who are more radiosensitive and can therefore potentially be used to adapt treatment. For example, CEST helped to predict the status of isocitrate dehydrogenase (IDH) mutation in patients with recently diagnosed untreated glioma. A, B, Amide proton transfer (APT) and downfield nuclear Overhauser effect (NOE)-suppressed (dns) APT (dns-APT) CEST metrics allowed prediction of isocitrate dehydrogenase mutation status with highest area under the curve (AUC) for the dns APT₉₀ metric (metric, 0.98) and a test sensitivity and specificity of 0.95 (95% CI: 0.77, 1.00) and 1.00 (95% CI: 0.59, 1.00), respectively ($P < .001$). Two example patients with newly diagnosed glioblastoma IDH-wt (c1–g1) and IDH-mut (c2–g2) are shown. C₁ shows gadolinium contrast-enhanced (Gdce) T1-weighted (T₁-w) MRI scans, and d₁ shows T2-weighted (T₂-w; turbo spin echo), relaxation-compensated multipool CEST MRI at 7.0-T with (e₁) separated APT, NOE (f₁), and dns-APT (g₁) effects. A ring-like hyperintensity can be delineated in the periphery of the IDH-wt glioblastoma at dns-APT imaging (g₁, white arrow), whereas the IDH-mut glioblastoma appears barely hyperintense at dns-APT (g₂, white arrow). The head of the caudate nucleus also appears hyperintense on dns-APT images (g₂, pink arrows). White arrows indicate the location of the tumor. Reprinted, with permission, from reference 62.

with MRI tumor features. For example, in patients with glioblastoma, an upregulated *PERIOSITIN* gene was shown to be associated with a high tumor volume at fluid-attenuated inversion recovery MRI (69). In breast cancer, luminal B subtypes were associated with contrast enhancement at

T1-weighted MRI (70). The association of imaging data and genomic data would potentially enable the construction of a model to predict outcome from imaging data. This model could be used to adapt treatment in the MRI linear accelerator on the basis of personalized genomic data.

DCE MRI and diffusion-weighted imaging are relatively mature methods and are likely to be, to our knowledge, the first quantitative MRI methods that will be used clinically with the MRI-linac (71). Initial implementation of DCE MRI and diffusion-weighted imaging on the Elekta 1.5-T MRI-linac demonstrated reproducible quantitative results on a phantom at four different institutions (72). CEST might be the next quantitative MRI method to be implemented, given its wide range of potential applications, particularly hypoxia imaging. Radiogenomics is in its early stages, and more studies will be required to demonstrate clinical impact.

Some anticipated gains of the use of the MRI-derived biomarkers we discussed include the following: dose painting (ie, delivery of higher doses to hypoxic regions) on the basis of imaging of hypoxia by using CEST and/or DCE MRI; improved target delineation on the basis of tissue cell density measured at diffusion-weighted imaging and/or T2 mapping; access to early treatment response assessment, which is expected to improve adaptation compared with anatomic imaging; and improved delineation of the lymphocytes-rich organs to decrease radiation-induced lymphopenia, which has the potential to increase treatment efficacy in combination with immunotherapy (73).

Key Developments in MRI for MRI-guided RT

There are key ongoing developments in MRI that will further facilitate advances in both offline and online, anatomic, and physiologic MRI-guided RT.

Flexible Radiation Transparent Receiver Coils

Diagnostic receiver coils are not optimized for offline MRI-guided RT. As we mentioned, the immobilization device increases the distance between the patient and the coil, resulting in signal-to-noise ratio losses. In online MRI-guided RT, the requirement to have radiation-transparent coils limits the number of elements, which results in signal-to-noise ratio losses and decreases in imaging speed. New developments that use high-impedance coils represent the future for coils in MRI-guided RT, promising flexible and radiation transparent coils with many elements (74).

Rapid MRI by Using Compressed Sensing and Artificial Intelligence

Despite the great advances in imaging speed, MRI is still slow compared with CT, resulting in prolonged offline simulation and online interfraction adaptation. The slow imaging speed of MRI also imposes limitations for real-time adaptive RT. The new generation of rapid MRI techniques acquire fewer data points (which is known as undersampling) and use previous information to reconstruct images with full information. Compressed sensing exploits the fact that images are compressible and has demonstrated significant acceleration in three-dimensional imaging and dynamic imaging (75–80). Most MRI manufacturers have translated compressed sensing to clinical practice. The technique is used in MRI-guided RT applications, particularly to reduce imaging time for three-di-

mensional imaging by up to 50% (81). Artificial intelligence techniques extend the ideas behind compressed sensing and train a convolutional neural network to map undersampled MRI data into images with full information by using hundreds or thousands of examples (82,83). Artificial intelligence–based fast MRI is only available as a research prototype, but MRI manufacturers are starting to implement the technique.

Motion-resolved MRI and Real-time Motion Imaging

Motion is often seen as a problem in MRI, and the conventional approach has been to avoid it in the acquisition. For example, breath-holds or respiratory gating are typically used, with the caveats of patient cooperation or acquisition inefficiency, respectively. Fast MRI techniques have been developed to capture real-time snapshots, but they are limited to two-dimensional imaging (84). An alternative approach is to capture motion and reconstruct motion states as a new dimension, such as with Extra Dimensional Golden Angle Radial Sparse MRI and MRI multi-tasking (85,86). Resolving motion rather than avoiding it could increase patient comfort and the efficiency of MRI simulation, and enable the use of MRI to adapt to volumetric motion in real time during treatment. Motion-resolved MRI is currently available as a research prototype with successful application to abdominal stereotactic body RT on the Elekta Unity MRI linear accelerator (87). Real-time volumetric motion imaging is being developed by several groups (32,88) and will enable a strategy for adaptive treatment in moving organs.

MRI Fingerprinting for Multiple Biomarker Mapping

A breakthrough in speed and accuracy in quantitative MRI is fingerprinting, which can capture multiple MRI tissue properties by using a single acquisition (89,90). MRI fingerprinting changes acquisition parameters in a random fashion so that each tissue generates a unique signal evolution. After the acquisition, a pattern recognition algorithm can find the set of MRI parameter values that best matches the acquired signal, just like a standard fingerprinting approach. The matching procedure uses Bloch equations, which result in more accurate modeling of the acquisition process. MRI fingerprinting is broadly available as a research prototype and one MRI manufacturer has implemented it as a commercial product. MRI fingerprinting has been successfully applied to monitor treatment response of brain tumors over several fractions in a quantitative manner (91). New developments that use MRI fingerprinting to image diffusion (92) and CEST (93) parameters with greater efficiency and robustness will be key in enabling all the benefits described in the above section on quantitative MRI biomarkers.

Clinical Trials

Early clinical trials of MRI-guided RT were focused on the use of MRI for treatment planning, particularly for prostate cancer. The main hypotheses tested were that the superior soft-tissue contrast of MRI would enable better target localization than CT, and that the dose distribution provided by MRI would be equivalent to that provided by CT. One of the first prospective clinical trials enrolled 48 patients with prostate cancer from a single institution and compared MRI-only

planning against planning with combined CT and MRI (2). The results of this clinical study demonstrated reproducible and superior target localization with the MRI-only approach compared with the combined CT and MRI approach. A larger multicenter and multivendor prospective clinical trial enrolled 170 patients with prostate cancer from four different institutions (94). The study included four different scanners and two different magnetic field strengths and compared dosimetric accuracy of MRI-only planning to CT planning. The overall mean dose differences between MRI and CT dose distributions were below 0.3% for all evaluated organs and targets. These early clinical trials demonstrated superior target delineation and equivalent dose distribution with MRI-only planning compared with CT planning.

Recent clinical trials evaluated the use of clinical MRI-linac systems for adaptive RT to enable hypofractionation and ablative doses with minimal toxicity in several anatomic sites affected by interfraction organ motion (eg, prostate) and intrafraction organ motion (eg, pancreas). The first prospective MRI-linac clinical trial enrolled 101 patients with intermediate- or high-risk prostate cancer. All patients underwent adaptive RT by using a ViewRay 0.35-T MRI-linac system in five fractions of 7.25 Gy (95). The trial did not use implanted markers, thereby eliminating an invasive procedure and potentially associated complications and implantation costs. Results after 3 months of treatment showed low toxicity, lower than originally expected. The maximum cumulative genitourinary and gastrointestinal toxicity were 23.8% (study hypothesis, 40%) and 5.0% (study hypothesis, 15%), respectively. A clinical trial, Multi-outcome Evaluation of Radiation Therapy Using the Unity MR-Linac Study, or MOMENTUM, on the basis of the Elekta 1.5-T Unity MRI-linac system was recently launched; it will enroll thousands of patients from several institutions (96).

Cost Considerations for MRI-guided RT

The final issues to be considered are cost, cost-benefit ratios, and cost-effectiveness. MRI-guided RT shows promise for improving the therapeutic ratio of RT. If this promise is realized, it is not unlikely that Markov models looking at the baseline cost as well as the cost of relapse and complications will identify subpopulations of patients who will benefit from MRI-guided RT. The following two evaluation approaches can be considered: (a) the traditional randomized trials that are ideal but in practice rarely performed for new technologies and not necessarily so-called isopose; and (b) model-based multifactorial decision-support systems built from large data sets and/or prospective cohort studies, an approach used for proton therapy (97). When evaluating the potential of MRI use in RT, it should ideally be considered that there are many innovations in physiologic imaging in addition to anatomic imaging that may lead to better personalized and adaptive treatment. It is however not yet clear which emerging imaging techniques will become standard and which will remain in the research domain. It is challenging to define the MRI techniques that will be used in real time and online (eg, to address daily changes in target geometry and/or biology) and which will be used mainly at the time of simulation or treatment evaluation offline. Given cost

considerations, for some applications, separate and dedicated systems may enable higher patient throughput. At present, the use of MRI-linac in routine clinical practice is limited to interfraction adaptation; however, we hope that as additional clinically relevant and unique applications emerge, evidence to quantify improvements in outcomes such as survival, toxicity, quality of life, or cost-effectiveness will become available. With the emergence of such evidence, we will witness another important step forward in targeting precision and the introduction of real-time adaptive RT.

Conclusion

MRI-guided radiation therapy (RT) promises to be the next big step in RT, overcoming the main limitations of CT guidance and offering opportunities for improved interfraction and intrafraction adaptation, dose accumulation mapping, and the use of MRI biomarkers. The developments we described in our review are illustrative of the convergence of life sciences, physical sciences, and engineering, which has been producing increasingly rapid innovation (98). Strong collaboration among radiation oncologists, radiologists, medical physicists, other imaging researchers and data scientists, engineers, and biologists is required to translate these developments to clinical RT on a broad scale. This may entail developing common education streams and research platforms into a multidisciplinary multicentric approach, which is singularly exemplified by the MRI-guided Linear Accelerator Consortium (99). We recommend reviewing research endeavors and training curricula to find effective ways for the radiology community to collaborate in multidisciplinary clinical research to advance clinical radiation oncology as efficiently and productively as possible. The MRI-guided Linear Accelerator Consortium would also be an ideal platform to validate the potential benefits of MRI-guided RT.

Acknowledgments: The authors thank members of the International Society for Strategic Studies in Radiology for active discussions. We thank Ada Mueller, MS, for editing and Drs Neelam Tyagi, Benjamin Knowles, Uulke van den Heide, Jan Lagendijk, and Simone Moorman for valuable suggestions.

Disclosures of Conflicts of Interest: **R.O.** Activities related to the present article: disclosed no relevant relationships. Activities not related to the present article: disclosed patent issued for GRASP technique and patent filed for MRSIGMA. Other relationships: disclosed no relevant relationships. **P.L.** Activities related to the present article: disclosed no relevant relationships. Activities not related to the present article: disclosed board memberships from Oncoradiomics SA, Convert Pharmaceuticals SA; consultancies from Benelux Health Ventures, ptTheragnostic-DNAmito, Convert Pharmaceuticals; grants/grants pending from Eurostars, the European Program SCANnTREAT, EuCanImage, Chameleon, Auto.Distinct, and NOW (Strategy); payments for lectures from Varian, Elekta; patents planned, pending, or issued; royalties from PCT/EP2014/059089; stock/stock options from Convert pharmaceuticals, the Medical Cloud Company, and Oncoradiomics; travel/accommodations/meeting expenses from Health Innovation Ventures; author discloses being a Licensee for Oncoradiomics. Other relationships: disclosed no relevant relationships. **J.P.P.** disclosed no relevant relationships. **M.E.L.** disclosed no relevant relationships. **H.P.S.** Activities related to the present article: disclosed grant from the large-scale equipment initiative of the German Research Council. Activities not related to the present article: disclosed payment for lectures from Siemens Healthineers, Bayer Healthcare; disclosed travel/accommodations/meeting expenses from Siemens Healthineers, Bayer Healthcare. Other relationships: disclosed no relevant relationships. **M.B.** Activities related to the present article: disclosed board membership from Merck; disclosed consultancy from HI-STEM (Heidelberg). Activities not related to the present article: disclosed grants/funding for research from Teutopharma, IBA, Bayer, Merck, Medipan; disclosed patents for DKFZ-PSMA617,

ANTIGEN PSMA, and similar IP portfolios; royalties from Elsevier (editor-in-chief honorarium for Radiotherapy and Oncology) and Oxford University Press (editor of Oxford Textbook of Oncology); disclosed other relationships from Bayer, Boehringer Ingelheim, Bosch, Roche, Siemens, IBA, Varian, Elekta, and Bruker. Other relationships: disclosed no relevant relationships. **H.H.** Activities related to the present article: disclosed no relevant relationships. Activities not related to the present article: disclosed compensation for board membership from Ion Beam Applications; service without compensation on External Advisory Board, Sidney Kimmel Comprehensive Cancer Center, Johns Hopkins; International Advisory Board, University of Vienna; Scientific Committee, DKFZ (German Cancer Research Center); Board of Trustees, DKFZ (German Cancer Research Center); and Scientific Advisory Board, Euro-BioImaging. Other relationships: disclosed no relevant relationships.

References

- Thompson MK, Poortmans P, Chalmers AJ, et al. Practice-changing radiation therapy trials for the treatment of cancer: where are we 150 years after the birth of Marie Curie? *Br J Cancer* 2018;119(4):389–407.
- Tyagi N, Fontenla S, Zelefsky M, et al. Clinical workflow for MR-only simulation and planning in prostate. *Radiat Oncol* 2017;12(1):119.
- Chen AM, Hsu S, Lamb J, et al. MRI-guided radiotherapy for head and neck cancer: initial clinical experience. *Clin Transl Oncol* 2018;20(2):160–168.
- Hunt A, Hansen VN, Oelfke U, Nill S, Hafeez S. Adaptive Radiotherapy Enabled by MRI Guidance. *Clin Oncol (R Coll Radiol)* 2018;30(11):711–719.
- Mutic S, Dempsey JF. The ViewRay system: magnetic resonance-guided and controlled radiotherapy. *Semin Radiat Oncol* 2014;24(3):196–199.
- Raaymakers BW, Lagendijk JJW, Overweg J, et al. Integrating a 1.5 T MRI scanner with a 6 MV accelerator: proof of concept. *Phys Med Biol* 2009;54(12):N229–N237.
- Fallone BG. The rotating biplanar linac-magnetic resonance imaging system. *Semin Radiat Oncol* 2014;24(3):200–202.
- Keall PJ, Barton M, Crozier S; Australian MRI-Linac Program, including contributors from Ingham Institute, Illawarra Cancer Care Centre, Liverpool Hospital, Stanford University, Universities of Newcastle, Queensland, Sydney, Western Sydney, and Wollongong. The Australian Magnetic Resonance Imaging-Linac Program. *Semin Radiat Oncol* 2014;24(3):203–206.
- Liney GP, Moerland MA. Magnetic resonance imaging acquisition techniques for radiotherapy planning. *Semin Radiat Oncol* 2014;24(3):160–168.
- Paulson ES, Erickson B, Schultz C, Allen Li X. Comprehensive MRI simulation methodology using a dedicated MRI scanner in radiation oncology for external beam radiation treatment planning. *Med Phys* 2015;42(1):28–39.
- McGee KP, Stormont RS, Lindsay SA, et al. Characterization and evaluation of a flexible MRI receive coil array for radiation therapy MR treatment planning using highly decoupled RF circuits. *Phys Med Biol* 2018;63(8):08NT02.
- Tyagi N, Zakian KL, Italiaander M, et al. Technical Note: A custom-designed flexible MR coil array for spine radiotherapy treatment planning. *Med Phys* 2020;47(7):3143–3152.
- Han X. MR-based synthetic CT generation using a deep convolutional neural network method. *Med Phys* 2017;44(4):1408–1419.
- Tyagi N, Fontenla S, Zhang J, et al. Dosimetric and workflow evaluation of first commercial synthetic CT software for clinical use in pelvis. *Phys Med Biol* 2017;62(8):2961–2975.
- Wiesinger F, Bylund M, Yang J, et al. Zero TE-based pseudo-CT image conversion in the head and its application in PET/MR attenuation correction and MR-guided radiation therapy planning. *Magn Reson Med* 2018;80(4):1440–1451.
- Usman M, Kakkar L, Matakos A, Kirkham A, Arridge S, Atkinson D. Joint B_0 and image estimation integrated with model based reconstruction for field map update and distortion correction in prostate diffusion MRI. *Magn Reson Imaging* 2020;65:90–99.
- Weygand J, Fuller CD, Ibbott GS, et al. Spatial Precision in Magnetic Resonance Imaging-Guided Radiation Therapy: The Role of Geometric Distortion. *Int J Radiat Oncol Biol Phys* 2016;95(4):1304–1316.
- Owrangi AM, Greer PB, Glide-Hurst CK. MRI-only treatment planning: benefits and challenges. *Phys Med Biol* 2018;63(5):05TR01.
- Pereira S, Pinto A, Alves V, Silva CA. Brain Tumor Segmentation Using Convolutional Neural Networks in MRI Images. *IEEE Trans Med Imaging* 2016;35(5):1240–1251.
- Njeh CF. Tumor delineation: The weakest link in the search for accuracy in radiotherapy. *J Med Phys* 2008;33(4):136–140.
- Létourneau D, Wong JW, Oldham M, et al. Cone-beam-CT guided radiation therapy: technical implementation. *Radiother Oncol* 2005;75(3):279–286.
- Oldham M, Létourneau D, Watt L, et al. Cone-beam-CT guided radiation therapy: A model for on-line application. *Radiother Oncol* 2005;75(3):271–278.
- Noel CE, Parikh PJ, Spencer CR, et al. Comparison of onboard low-field magnetic resonance imaging versus onboard computed tomography for anatomy visualization in radiotherapy. *Acta Oncol* 2015;54(9):1474–1482.
- Oh S, Stewart J, Moseley J, et al. Hybrid adaptive radiotherapy with on-line MRI in cervix cancer IMRT. *Radiother Oncol* 2014;110(2):323–328.
- Fast MF, Krauss A, Oelfke U, Nill S. Position detection accuracy of a novel linac-mounted intrafractional x-ray imaging system. *Med Phys* 2012;39(1):109–118.
- Keall PJ, Sawant A, Cho B, et al. Electromagnetic-guided dynamic multileaf collimator tracking enables motion management for intensity-modulated arc therapy. *Int J Radiat Oncol Biol Phys* 2011;79(1):312–320.
- Pollard JM, Wen Z, Sadagopan R, Wang J, Ibbott GS. The future of image-guided radiotherapy will be MR guided. *Br J Radiol* 2017;90(1073):20160667.
- Doemer A, Chetty IJ, Glide-Hurst C, et al. Evaluating organ delineation, dose calculation and daily localization in an open-MRI simulation workflow for prostate cancer patients. *Radiat Oncol* 2015;10(1):37.
- Crane CH, O'Reilly EM. Ablative Radiotherapy Doses for Locally Advanced: Pancreatic Cancer (LAPC). *Cancer J* 2017;23(6):350–354.
- Finazzi T, van Sörnsen de Koste JR, Palacios MA, et al. Delivery of magnetic resonance-guided single-fraction stereotactic lung radiotherapy. *Phys Imaging Radiat Oncol* 2020;14:P17–P23.
- Glitzner M, Woodhead PL, Borman PTS, Lagendijk JJW, Raaymakers BW. Technical note: MLC-tracking performance on the Elekta unity MRI-linac. *Phys Med Biol* 2019;64(15):15NT02.
- Feng L, Tyagi N, Otazo R. MRSIGMA: Magnetic Resonance SIGNature MAtching for real-time volumetric imaging. *Magn Reson Med* 2020;84(3):1280–1292.
- Huttinga NRF, van den Berg CAT, Luijten PR, Sbrizzi A. MR-MOTUS: model-based non-rigid motion estimation for MR-guided radiotherapy using a reference image and minimal k-space data. *Phys Med Biol* 2020;65(1):015004.
- Borman PTS, Bos C, Stemkens B, Moonen CTW, Raaymakers BW, Tijssen RHN. Assessment of 3D motion modeling performance for dose accumulation mapping on the MR-linac by simultaneous multislice MRI. *Phys Med Biol* 2019;64(9):095004.
- Glitzner M, Crijns SPM, de Senneville BD, et al. On-line MR imaging for dose validation of abdominal radiotherapy. *Phys Med Biol* 2015;60(22):8869–8883.
- Thames HD, Hendry JH. Fractionation in Radiotherapy. London, England: Taylor & Francis, 1987.
- Lühr A, von Neubeck C, Pawelke J, et al. “Radiobiology of Proton Therapy”: Results of an international expert workshop. *Radiother Oncol* 2018;128(1):56–67.
- Marks LB, Yorke ED, Jackson A, et al. Use of normal tissue complication probability models in the clinic. *Int J Radiat Oncol Biol Phys* 2010;76(3 Suppl):S10–S19.
- Bentzen SM, Constine LS, Deasy JO, et al. Quantitative Analyses of Normal Tissue Effects in the Clinic (QUANTEC): an introduction to the scientific issues. *Int J Radiat Oncol Biol Phys* 2010;76(3 Suppl):S3–S9.
- Knowles BR, Friedrich F, Fischer C, Paech D, Ladd ME. Beyond T2 and 3T: New MRI techniques for clinicians. *Clin Transl Radiat Oncol* 2019;18:87–97.
- Raaijmakers AJ, Raaymakers BW, Lagendijk JJ. Integrating a MRI scanner with a 6 MV radiotherapy accelerator: dose increase at tissue-air interfaces in a lateral magnetic field due to returning electrons. *Phys Med Biol* 2005;50(7):1363–1376.
- Raaijmakers AJE, Raaymakers BW, Lagendijk JJW. Magnetic-field-induced dose effects in MR-guided radiotherapy systems: dependence on the magnetic field strength. *Phys Med Biol* 2008;53(4):909–923.
- Das IJMK, McGee KP, Tyagi N, Wang H. Role and future of MRI in radiation oncology. *Br J Radiol* 2019;92(1094):20180505.
- Baumann M, Krause M, Overgaard J, et al. Radiation oncology in the era of precision medicine. *Nat Rev Cancer* 2016;16(4):234–249.
- Cao Y. The promise of dynamic contrast-enhanced imaging in radiation therapy. *Semin Radiat Oncol* 2011;21(2):147–156.
- Bisdas S, Naegele T, Ritz R, et al. Distinguishing recurrent high-grade gliomas from radiation injury: a pilot study using dynamic contrast-enhanced MR imaging. *Acad Radiol* 2011;18(5):575–583.
- Zahra MA, Tan LT, Priest AN, et al. Semiquantitative and quantitative dynamic contrast-enhanced magnetic resonance imaging measurements predict radiation response in cervix cancer. *Int J Radiat Oncol Biol Phys* 2009;74(3):766–773.
- Galbán CJ, Mukherji SK, Chenevert TL, et al. A feasibility study of parametric response map analysis of diffusion-weighted magnetic resonance imaging scans of head and neck cancer patients for providing early detection of therapeutic efficacy. *Transl Oncol* 2009;2(3):184–190.
- Liu L, Wu N, Ouyang H, Dai JR, Wang WH. Diffusion-weighted MRI in early assessment of tumour response to radiotherapy in high-risk prostate cancer. *Br J Radiol* 2014;87(1043):20140359.
- Foltz WD, Wu A, Chung P, et al. Changes in apparent diffusion coefficient and T2 relaxation during radiotherapy for prostate cancer. *J Magn Reson Imaging* 2013;37(4):909–916.
- van Zijl PC, Yadav NN. Chemical exchange saturation transfer (CEST): what is in a name and what isn't? *Magn Reson Med* 2011;65(4):927–948.

52. Ma B, Blakeley JO, Hong X, et al. Applying amide proton transfer-weighted MRI to distinguish pseudoprogression from true progression in malignant gliomas. *J Magn Reson Imaging* 2016;44(2):456–462.
53. Harris RJ, Cloughesy TF, Liau LM, et al. pH-weighted molecular imaging of gliomas using amine chemical exchange saturation transfer MRI. *Neuro Oncol* 2015;17(11):1514–1524.
54. Overgaard J, Horsman MR. Modification of hypoxia-induced radioresistance in tumors by the use of oxygen and sensitizers. *Semin Radiat Oncol* 1996;6(1):10–21.
55. Yaromina A, Thames H, Zhou X, et al. Radiobiological hypoxia, histological parameters of tumour microenvironment and local tumour control after fractionated irradiation. *Radiother Oncol* 2010;96(1):116–122.
56. Ladd ME, Bachert P, Meyerspeer M, et al. Pros and cons of ultra-high-field MRI/MRS for human application. *Prog Nucl Magn Reson Spectrosc* 2018;109:1–50.
57. Do QN, Ratnakar JS, Kovács Z, Sherry AD. Redox- and hypoxia-responsive MRI contrast agents. *ChemMedChem* 2014;9(6):1116–1129.
58. Poser BA, Norris DG. Fast spin echo sequences for BOLD functional MRI. *MAGMA* 2007;20(1):11–17.
59. Press RH, Shu HG, Shim H, et al. The Use of Quantitative Imaging in Radiation Oncology: A Quantitative Imaging Network (QIN) Perspective. *Int J Radiat Oncol Biol Phys* 2018;102(4):1219–1235.
60. Grimes DR, Warren DR, Warren S. Hypoxia imaging and radiotherapy: bridging the resolution gap. *Br J Radiol* 2017;90(1076):20160939.
61. Noman MZ, Hasmim M, Lequeux A, et al. Improving Cancer Immunotherapy by Targeting the Hypoxic Tumor Microenvironment: New Opportunities and Challenges. *Cells* 2019;8(9):E1083.
62. Paech D, Windschuh J, Oberhollenzer J, et al. Assessing the predictability of IDH mutation and MGMT methylation status in glioma patients using relaxation-compensated multipool CEST MRI at 7.0 T. *Neuro Oncol* 2018;20(12):1661–1671.
63. Quennet V, Yaromina A, Zips D, et al. Tumor lactate content predicts for response to fractionated irradiation of human squamous cell carcinomas in nude mice. *Radiother Oncol* 2006;81(2):130–135.
64. Oz G, Alger JR, Barker PB, et al. Clinical proton MR spectroscopy in central nervous system disorders. *Radiology* 2014;270(3):658–679.
65. Kurhanewicz J, Vigneron DB, Ardenkjaer-Larsen JH, et al. Hyperpolarized ¹³C MRI: Path to Clinical Translation in Oncology. *Neoplasia* 2019;21(1):1–16.
66. Gallagher FA, Woitek R, McLean MA, et al. Imaging breast cancer using hyperpolarized carbon-13 MRI. *Proc Natl Acad Sci U S A* 2020;117(4):2092–2098.
67. Granlund KL, Tee SS, Vargas HA, et al. Hyperpolarized MRI of Human Prostate Cancer Reveals Increased Lactate with Tumor Grade Driven by Monocarboxylate Transporter 1. *Cell Metab* 2020;31(1):105–114.e3.
68. Mazurowski MA. Radiogenomics: what it is and why it is important. *J Am Coll Radiol* 2015;12(8):862–866.
69. Zinn PO, Mahajan B, Sathyan P, et al. Radiogenomic mapping of edema/cellular invasion MRI-phenotypes in glioblastoma multiforme. *PLoS One* 2011;6(10):e25451.
70. Mazurowski MA, Zhang J, Grimm LJ, Yoon SC, Silber JI. Radiogenomic analysis of breast cancer: luminal B molecular subtype is associated with enhancement dynamics at MR imaging. *Radiology* 2014;273(2):365–372.
71. Datta A, Aznar MC, Dubec M, Parker GJM, O'Connor JPB. Delivering Functional Imaging on the MRI-Linac: Current Challenges and Potential Solutions. *Clin Oncol (R Coll Radiol)* 2018;30(11):702–710.
72. Kooreman ES, van Houdt PJ, Nowee ME, et al. Feasibility and accuracy of quantitative imaging on a 1.5 T MR-linear accelerator. *Radiother Oncol* 2019;133:156–162.
73. Grassberger C, Hong TS, Hato T, et al. Differential Association Between Circulating Lymphocyte Populations With Outcome After Radiation Therapy in Subtypes of Liver Cancer. *Int J Radiat Oncol Biol Phys* 2018;101(5):1222–1225.
74. Zijlema SE, Tijssen RHN, Malkov VN, et al. Design and feasibility of a flexible, on-body, high impedance coil receive array for a 1.5 T MR-linac. *Phys Med Biol* 2019;64(18):185004.
75. Candes EJ, Romberg J, Tao T. Robust uncertainty principles: Exact signal reconstruction from highly incomplete frequency information. *IEEE Trans Inf Theory* 2006;52(2):489–509.
76. Lustig M, Donoho D, Pauly JM. Sparse MRI: The application of compressed sensing for rapid MR imaging. *Magn Reson Med* 2007;58(6):1182–1195.
77. Chandarana H, Doshi AM, Shanbhogue A, et al. Three-dimensional MR Cholangiopancreatography in a Breath Hold with Sparsity-based Reconstruction of Highly Undersampled Data. *Radiology* 2016;280(2):585–594.
78. Zhang T, Cheng JY, Potnick AG, et al. Fast pediatric 3D free-breathing abdominal dynamic contrast enhanced MRI with high spatiotemporal resolution. *J Magn Reson Imaging* 2015;41(2):460–473.
79. Feng L, Grimm R, Block KT, et al. Golden-angle radial sparse parallel MRI: combination of compressed sensing, parallel imaging, and golden-angle radial sampling for fast and flexible dynamic volumetric MRI. *Magn Reson Med* 2014;72(3):707–717.
80. Otazo R, Kim D, Axel L, Sodickson DK. Combination of compressed sensing and parallel imaging for highly accelerated first-pass cardiac perfusion MRI. *Magn Reson Med* 2010;64(3):767–776.
81. Gao Y, Zhou Z, Han F, et al. Accelerated 3D bSSFP imaging for treatment planning on an MRI-guided radiotherapy system. *Med Phys* 2018;45(6):2595–2602.
82. Hammernik K, Klatzer T, Kobler E, et al. Learning a variational network for reconstruction of accelerated MRI data. *Magn Reson Med* 2018;79(6):3055–3071.
83. Zhu B, Liu JZ, Cauley SF, Rosen BR, Rosen MS. Image reconstruction by domain-transform manifold learning. *Nature* 2018;555(7697):487–492.
84. Uecker M, Zhang S, Voit D, Karaus A, Merboldt KD, Frahm J. Real-time MRI at a resolution of 20 ms. *NMR Biomed* 2010;23(8):986–994.
85. Christodoulou AG, Shaw JL, Nguyen C, et al. Magnetic resonance multitasking for motion-resolved quantitative cardiovascular imaging. *Nat Biomed Eng* 2018;2(4):215–226.
86. Feng L, Axel L, Chandarana H, Block KT, Sodickson DK, Otazo R. XD-GRASP: Golden-angle radial MRI with reconstruction of extra motion-state dimensions using compressed sensing. *Magn Reson Med* 2016;75(2):775–788.
87. Paulson ES, Ahunbay E, Chen X, et al. 4D-MRI driven MR-guided online adaptive radiotherapy for abdominal stereotactic body radiation therapy on a high field MR-Linac: Implementation and initial clinical experience. *Clin Transl Radiat Oncol* 2020;23:72–79.
88. Bruijnen T, Stemkens B, Lagendijk JJW, van den Berg CAT, Tijssen RHN. Multiresolution radial MRI to reduce IDLE time in pre-beam imaging on an MR-Linac (MR-RIDDLE). *Phys Med Biol* 2019;64(5):055011.
89. Ma D, Gulani V, Seiberlich N, et al. Magnetic resonance fingerprinting. *Nature* 2013;495(7440):187–192.
90. Badve C, Yu A, Dastmalchian S, et al. MR Fingerprinting of Adult Brain Tumors: Initial Experience. *AJNR Am J Neuroradiol* 2017;38(3):492–499.
91. Lu L, Chen Y, Shen C, et al. Initial assessment of 3D magnetic resonance fingerprinting (MRF) towards quantitative brain imaging for radiation therapy. *Med Phys* 2020;47(3):1199–1214.
92. Yu AC, Badve C, Ponsky LE, et al. Development of a Combined MR Fingerprinting and Diffusion Examination for Prostate Cancer. *Radiology* 2017;283(3):729–738.
93. Cohen O, Huang S, McMahon MT, Rosen MS, Farrar CT. Rapid and quantitative chemical exchange saturation transfer (CEST) imaging with magnetic resonance fingerprinting (MRF). *Magn Reson Med* 2018;80(6):2449–2463.
94. Persson E, Gustafsson C, Nordström F, et al. MR-OPERA: A Multicenter/Multivendor Validation of Magnetic Resonance Imaging-Only Prostate Treatment Planning Using Synthetic Computed Tomography Images. *Int J Radiat Oncol Biol Phys* 2017;99(3):692–700.
95. Bruynzeel AME, Tetar SU, Oei SS, et al. A Prospective Single-Arm Phase 2 Study of Stereotactic Magnetic Resonance Guided Adaptive Radiation Therapy for Prostate Cancer: Early Toxicity Results. *Int J Radiat Oncol Biol Phys* 2019;105(5):1086–1094.
96. The MOMENTUM Study: The Multiple Outcome Evaluation of Radiation Therapy Using the MR-Linac Study (MOMENTUM). [ClinicalTrials.gov. https://clinicaltrials.gov/ct2/show/NCT04075305](https://clinicaltrials.gov/ct2/show/NCT04075305). Accessed September 1, 2020.
97. Cheng Q, Roelofs E, Ramaekers BL, et al. Development and evaluation of an online three-level proton vs photon decision support prototype for head and neck cancer - Comparison of dose, toxicity and cost-effectiveness. *Radiother Oncol* 2016;118(2):281–285.
98. Hricak H. 2016 New Horizons Lecture: Beyond Imaging-Radiology of Tomorrow. *Radiology* 2018;286(3):764–775.
99. Kerkmeijer LGW, Fuller CD, Verkooijen HM, et al. The MRI-Linear Accelerator Consortium: Evidence-Based Clinical Introduction of an Innovation in Radiation Oncology Connecting Researchers, Methodology, Data Collection, Quality Assurance, and Technical Development. *Front Oncol* 2016;6:215.